Title

Evolving membrane-associated accessory protein variants for improved adeno-associated virus production.

Journal

Molecular Therapy, 32(2)

Authors

Schieferecke, Adam

Lee, Hyuncheol

Chen, Aleysha

et al.

Publication Date

2024-02-07

DOI

10.1016/j.ymthe.2023.12.015

Peer reviewed

Molecular Therapy
Original Article

Evolving membrane-associated accessory protein variants for improved adeno-associated virus production

Adam J. Schieferecke,[1,2,6] Hyuncheol Lee,[2,6] Aleysha Chen,[3] Vindhya Kilaru,[3] Justin Krish Williams,[1] and David V. Schaffer[1,2,3,4,5]

[1]Department of Molecular and Cell Biology, University of California, Berkeley, Berkeley, CA 94720, USA; [2]California Institute for Quantitative Biosciences, University of California, Berkeley, Berkeley, CA 94720, USA; [3]Department of Bioengineering, University of California, Berkeley, Berkeley, CA 94720, USA; [4]Department of Chemical and Biomolecular Engineering, University of California, Berkeley, Berkeley, CA 94720, USA; [5]Helen Wills Neuroscience Institute, University of California, Berkeley, Berkeley, CA 94720, USA

Manufacturing sufficient adeno-associated virus (AAV) to meet current and projected clinical needs is a significant hurdle to the growing gene therapy industry. The recently discovered membrane-associated accessory protein (MAAP) is encoded by an alternative open reading frame in the AAV *cap* gene that is found in all presently reported natural serotypes. Recent evidence has emerged supporting a functional role of MAAP in AAV egress, although the underlying mechanisms of MAAP function remain unknown. Here, we show that inactivation of MAAP from AAV2 by a single point mutation that is silent in the VP1 open reading frame (ORF) (AAV2-ΔMAAP) decreased exosome-associated and secreted vector genome production. We hypothesized that novel MAAP variants could be evolved to increase AAV production and thus subjected a library encoding over 1×10^6 MAAP protein variants to five rounds of packaging selection into the AAV2-ΔMAAP capsid. Between each successive packaging round, we observed a progressive increase in both overall titer and ratio of secreted vector genomes conferred by the bulk-selected MAAP library population. Next-generation sequencing uncovered enriched mutational features, and a resulting selected MAAP variant containing missense mutations and a frame-shifted C-terminal domain increased overall GFP transgene packaging in AAV2, AAV6, and AAV9 capsids.

INTRODUCTION

Adeno-associated virus (AAV) is a dependoparvovirus whose natural genome contains ~4.7 kb of single-stranded DNA (ssDNA) that is flanked by inverted terminal repeats (ITRs) and encodes up to 10 known proteins in a highly overlapped fashion.[1–3] The *rep* gene encodes four protein products named according to their molecular weight: Rep78 and Rep68 perform important functions related to cell cycle modulation,[4,5] transcriptional activation,[6,7] and genomic replication,[8,9] whereas Rep52 and Rep40 play essential roles in loading nascent ssDNA genomes into assembled capsids.[10,11] Downstream of *rep* lies the *cap* region, which includes open reading frames (ORFs) that encode up to six known protein products: VP1, VP2, and VP3 are structural proteins that assemble to form the capsid[12,13]; the assembly activating protein (AAP) targets VP proteins to the nucleus and is involved in capsid assembly[14–16]; the X protein is found in most natural AAV serotypes, although its function and underlying mechanisms are yet to be fully elucidated[17,18]; and the membrane-associated accessory protein (MAAP) yields a 13-kDa protein product encoded by a +1 ORF that is found in all presently reported natural serotypes.[3] In addition, AAV requires the function of helper genes from larger viruses such as adenoviruses or herpesviruses to complete its replication cycle.[1,19–21]

AAVs offer multiple advantageous properties for use as clinical gene delivery vectors, including the ability to package heterologous genetic payloads enabled by providing natural viral *rep* and *cap* genes in *trans* of an ITR-containing vector genome,[2,22] inherent non-pathogenicity, and relatively low immunogenicity in humans leading to an extensive clinical safety profile,[23–25] long-term episomal expression with low risk of genomic integration,[26,27] established techniques to produce vectors in cell culture,[28,29] physical stability,[30,31] efficient transduction of both dividing and non-dividing cells,[32,33] and engineerable tropism for specific cell types.[33,34] Accordingly, AAVs are the subject of 161 active- or recruiting-status clinical trials[25] and five US Food and Drug Administration (FDA)-approved products as of October, 2023.[35–39] As the number of clinical-stage AAV products increases, manufacturing the high quantities of good manufacturing practice (GMP)-grade AAV necessary to address current and especially future clinical dosing needs presents a significant challenge.[40,41]

First reported in 2019, MAAP initiates translation at a CTG codon in the +1 ORF relative to the VP1 ORF,[3,42] associates with the plasma

Received 23 June 2023; accepted 14 December 2023;
https://doi.org/10.1016/j.ymthe.2023.12.015.

[6]These authors contributed equally

Correspondence: David V. Schaffer, PhD, Department of Chemical and Biomolecular Engineering, University of California, Berkeley, Berkeley, CA 94720, USA.
E-mail: schaffer@berkeley.edu

membrane,[3,43] and increases AAV2 packaging fitness through competitive exclusion as indicated by wild-type (WT) AAV2 outcompeting MAAP-null AAV2 in co-infection assays.[3] Recently, evidence supporting a functional role for MAAP in AAV secretion has emerged, including observations that ablating MAAP reduces AAV8 secretion levels, *trans*-complementation of AAV8 MAAP can rescue secretion levels across several different AAV serotypes, and AAV8 MAAP interacts with the surface of extracellular vesicles (EVs).[43] Furthermore, C-terminal MAAP truncations have been shown to confer a modest increase in AAV2 or AAV8 vector genome production.[42,43]

Here, we show that ablation of MAAP decreased both EV-associated and secreted AAV2 vector genome titers, further confirming its role in AAV egress. Furthermore, we postulated that directed evolution, diversification of a target gene followed by selection for improved function, could be utilized to engineer MAAP variants that confer increased recombinant AAV packaging in HEK293 cells. To test this hypothesis, we generated an error-prone PCR library of over 1×10^6 MAAP variants, which were subjected to five rounds of iterative packaging into an AAV2 capsid using a *cap* gene in which MAAP expression was inactivated (AAV2-ΔMAAP). With each successive packaging round, we observed a progressive increase in both overall titer and ratio of secreted vector genomes conferred by the bulk-selected MAAP library population. Next-generation sequencing (NGS) revealed mutational features, including novel C-terminal domains. When stably expressed in HEK293 cells, leading selected MAAP variants increased packaging of a GFP transgene into AAV2, AAV6, or AAV9 capsids. Our results contribute new insights into AAV biology, describe a broadly useful directed evolution strategy for engineering non-structural AAV genes, and uncover novel MAAP variants with potential to improve upstream recombinant AAV manufacturing.

RESULTS

MAAP is an important factor for AAV2 secretion

It was recently shown that MAAP affects the kinetics and quantity of AAV8 secretion.[43] To confirm the effect of MAAP on the production of AAV2, we generated an AAV2 genome from which the endogenous expression of MAAP was ablated (AAV2-ΔMAAP) by introducing a point mutation that results in an early stop codon at the 19th leucine of MAAP but is silent in the overlapping VP1 ORF (Figures S1A and S1B). We packaged AAV2-ΔMAAP in HEK293 cells and sampled the supernatant and cell lysate fractions 72 h post transfection. We observed a marked decrease in the number of vector genomes of AAV2-ΔMAAP secreted into the supernatant relative to WT AAV2 (Figures 1A and 1B). Restoration of MAAP expression from a plasmid in *trans* partially rescued the titer of AAV2 secreted in cellular supernatant (Figures 1A and 1B). Notably, a statistically significant difference was not observed in the ratio of vector genomes per capsid between WT AAV2 and AAV2-ΔMAAP associated with cells or supernatant, suggesting that the role that natural MAAP plays in AAV2 production is independent of capsid genome loading (Figures 1C–1E).

Ablation of MAAP decreases AAV2 association with EVs

To directly analyze the effects of MAAP inactivation on the secreted AAV population, EVs from HEK293 cells transfected with pHelper plus either AAV2 or AAV2-ΔMAAP were isolated into individual fractions, which underwent quantification and molecular profiling via western blot staining for EV-associated viral and cellular proteins (Figures 2A and 2B). Specifically, following a series of collections and centrifugations of supernatant samples from AAV transfection cultures, the aggregate crude pellet was suspended and floated to the interface between 40% and 55% sucrose in a step gradient and then fractionated, wherein the first five fractions were stained for protein markers and analyzed for counts of EV particles and EV-associated AAV2 titers (Figure 2A). Notably, lower levels of EVs were secreted from AAV2-ΔMAAP-transfected cell lines compared to cells not producing AAV (Figures 2B and 2C). Although cells producing AAV2ΔMAAP showed no statistically significant difference in the levels of EVs produced relative to cells producing AAV2 for which MAAP was intact (Figure 2D), the AAV vector genomes and capsid proteins associated with isolated EV fractions were lower for AAVΔMAAP vs. WT AAV2 samples (Figures 2E and 2F). These results indicate that MAAP promotes AAV secretion, at least in part, through the association of AAV with EVs.

Directed evolution of MAAP results in increased AAV2 production and strong enrichment of unique variants

Directed evolution is an especially powerful approach for engineering proteins for which underlying mechanistic knowledge is insufficient to enable rational design, such as for the recently discovered MAAP. Based on recent evidence reported by other groups[3,42,43] and our own data (Figures 1 and 2), we hypothesized that directed evolution could yield novel MAAP variants that improve AAV production in industrially relevant cell lines. To test this idea, we generated an error-prone PCR library encoding over 1×10^6 MAAP protein variants, which we incorporated downstream of a cytomegalovirus (CMV) promoter and flanked by AAV2 ITRs in a plasmid called pMAAP-Library (Figure 3A). The resulting MAAP library was packaged into AAV2 capsids in HEK293 cells by co-transfection with pHelper and a plasmid containing the *rep* and *cap* genes in which endogenous MAAP was inactivated (pAAV2-ΔMAAP). The AAV2-packaged MAAP library was subsequently used for iterative rounds of supernatant-based selection as described in Figure 3A and the section "materials and methods." Briefly, pMAAP-Library, pHelper, and pAAV2-ΔMAAP were triple transfected into HEK293 cells and incubated for 96 h, at which point secreted AAV2-ΔMAAP was sampled by removing the cells from the supernatant, titered by qPCR, and infected onto fresh HEK293 cells at MOI = 100 for the subsequent round of packaging with the assistance of co-transfected pHelper and pAAV-ΔMAAP, a process that was iterated four times. The use of MOI = 100, calculated based on vector genome number, is known to result in successful transduction of <20% of cells,[33] an assumption we confirmed empirically in our HEK293 cell cultures prior to performing selection (A.J.S. and H.L., unpublished data). The bulk-selected MAAP library population was titered for each successive selection round and showed a progressive and significant increase in both overall titer and

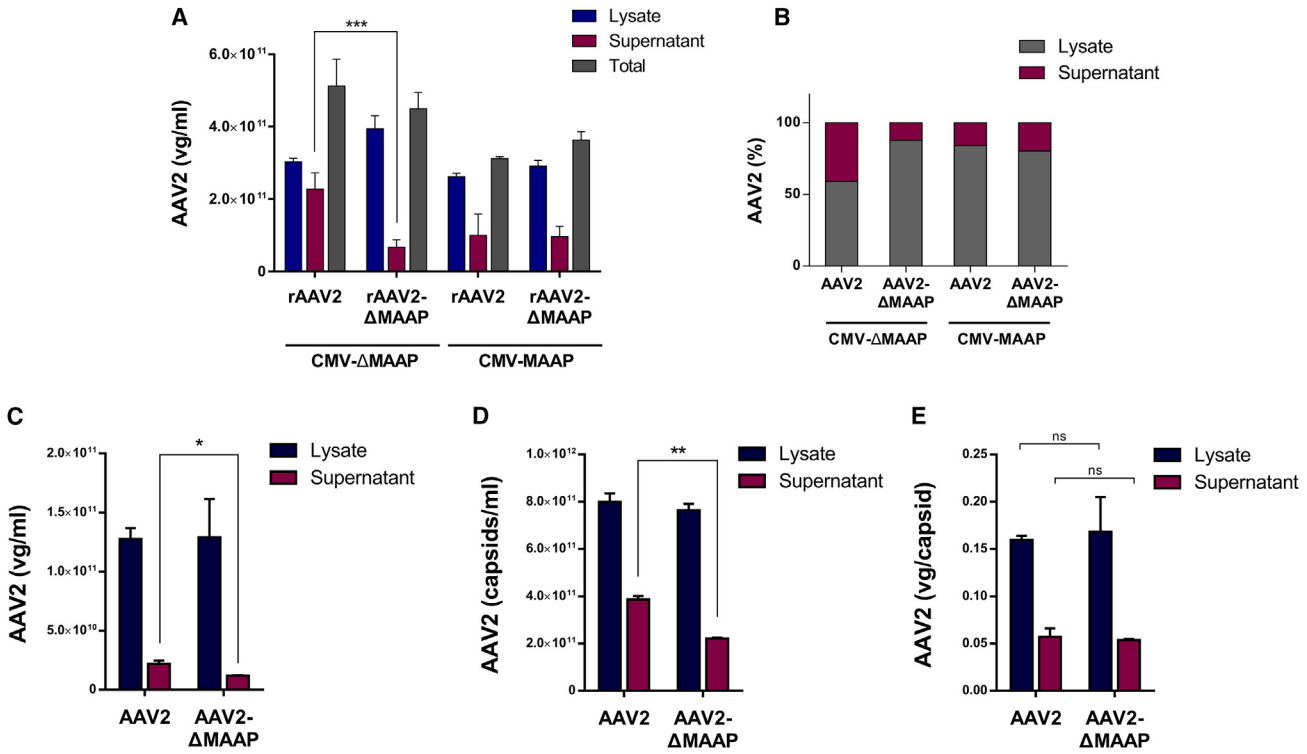

Figure 1. AAV2 MAAP affects viral secretion

(A) Knockout of MAAP from AAV2 increased proportion of vector genomes retained in the cell (lysate) 72 h post transfection as shown by qPCR. Navy blue, cell-associated (lysate) AAV2 titer; maroon, supernatant-associated (secreted) AAV titer; gray, total AAV titer. The inactivation of MAAP resulted in decreased secretion (more AAV retained within the cell). (B) Same data as in (A) showing the ratio of secreted AAV2 (maroon) vs. intracellular AAV2 (gray). (C) ELISA of AAV2 capsids present in the cell-associated (lysate) or supernatant fractions. (D) Secreted AAV2 capsid levels produced in the presence or absence of MAAP. (E) Vector genome/capsid ratios of the data depicted in parts (C) and (D). All data are representative of at least two independent experiments. Error bars, mean ± SD. *$p < 0.05$, **$p < 0.01$, *** < 0.005 (Student's t test, two sampled).

the ratio of secreted vector genomes present in the supernatant (from 15.8% to 60.0%) with each round. (Figures 3B and 3C). Following four selection rounds, we performed a head-to-head comparison of AAV2 production levels conferred by WT AAV2 MAAP (MAAP-WT2), empty vector (no MAAP), or the bulk-selected MAAP library population, each packaged into AAV2 capsids produced from pAAV2Δ MAAP (Figure 3D). Encouragingly, the bulk-selected MAAP library population exhibited over a 2-fold increase in overall titer (Figure 3E) and an increase in the relative level of AAV associated with cells vs. supernatant (84.9%, 48.6%, or 33.5% AAV found in culture medium for the bulk-selected library, MAAP-WT2, or MAAP-null conditions, respectively; Figure 3F). NGS of the pre- vs. post-selected populations showed both a decrease in the overall number of unique MAAP variants and an increase in the frequency of specific variants (Figure 4A). Due to MAAP's small coding sequence size of 360 nucleic acids, an individual 300 paired-end Illumina read can encompass a full MAAP coding sequence, and the resulting full-length MAAP sequences were translated into amino acid sequences. Individual amino acid sequences were enriched up to 697-fold relative to their prevalence in the pre-selected library population (Figure 4C). Interestingly, we observed strong enrichment of early stop codons in the post-selected MAAP dataset (Figure 4B), a result that corroborates recent findings that truncated MAAP sequences increase secreted AAV8 or AAV2 levels.[42,43] However, additional common mutational features, importantly including missense mutations as well as frameshifts that resulted in novel C-terminal domains (Figure 4D; Table S1), were also enriched on the amino acid level (Figures 4C and 4D).

Isolated MAAP variants confer increased recombinant AAV2 packaging

We next determined whether individual MAAP variants enriched in the post-selected population were responsible for the observed increase in AAV2 packaging and secretion (Figure 3). Two MAAP clones encompassing some of the most enriched mutational features observed in the NGS dataset and chosen based on their order of enrichment were selected for head-to-head comparisons of their effect on AAV2 packaging (Figures 4B and 4D; Table S1). For example, MAAP-SL08 was a fundamentally novel variant that contained the first 26 amino acids of MAAP-WT2 (normally 119 amino acids in length) followed by a frameshift into the VP1 amino acid positions 54–196 with nine missense mutations scattered three to 20 amino acids apart (Figure 4D; Table S1). By comparison, the most enriched variant in the dataset, SL01, contained the first 73 amino acids of MAAP-WT2 with the exceptions of 13 missense

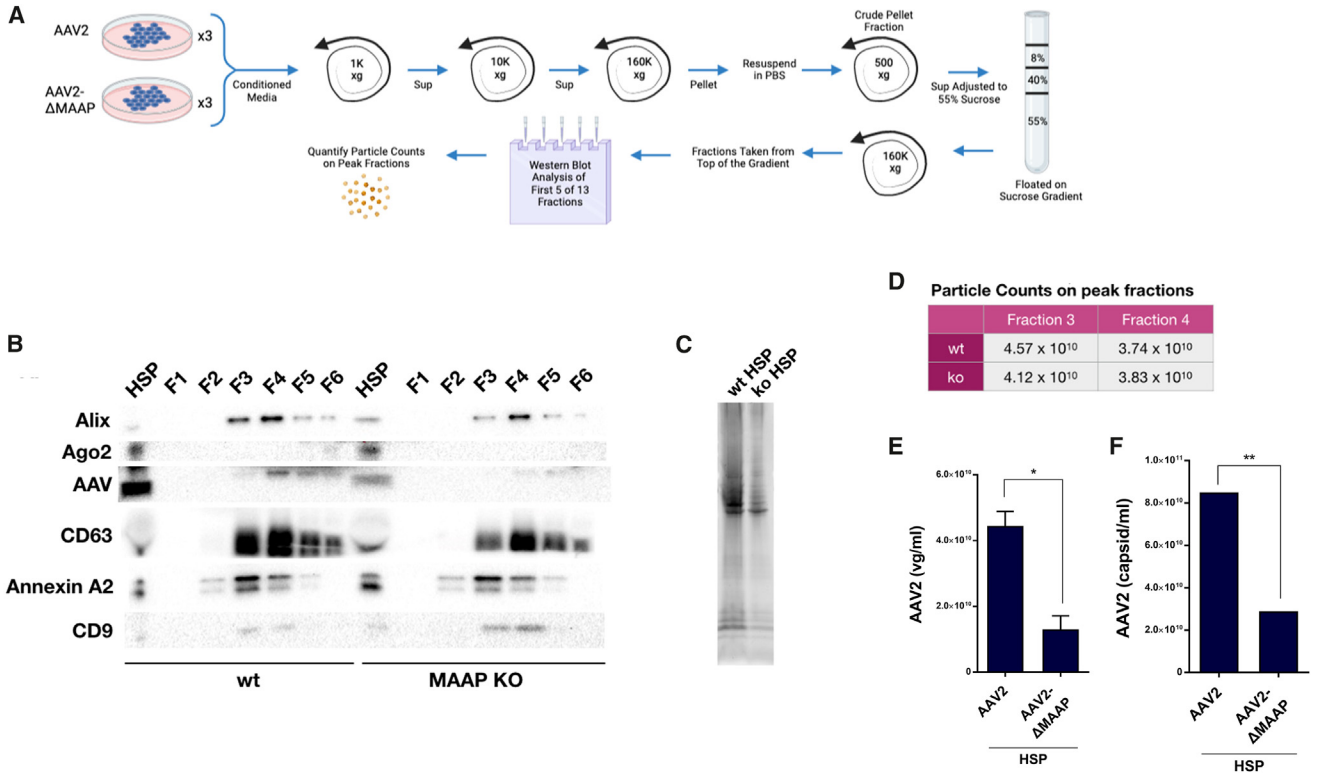

Figure 2. MAAP is required for optimal AAV2 association with exosomes

(A–C) AAV-GFP was packaged with AAV2-WT or AAV2-MAAP-null packaging plasmids in HEK293 cells. Cell culture medium was changed with exosome-free DMEM at 1 day post transfection and supernatant was harvested at 3 days post transfection for exosome analysis. Schematic showing the process for isolating and analyzing exosomes is shown in (A) and was created on BioRender.com. Immunoblot of exosome markers and AAV capsid protein in each fraction is shown in (B). (D) EV particle counts were unaffected by the presence or absence of MAAP. (E and F) qPCR-based vector genome titer (E) and capsid ELISA (F) to quantify EV-associated AAV2. Data are representative of two independent experiments (E and F). Error bars, mean ± SD. *$p < 0.05$, **$p < 0.01$ (Student's t test, two sampled).

mutations followed by a frameshift mutation that resulted in a novel 26 amino acid-long C-terminal domain (Figure 4D; Table S1). It was recently reported that truncated MAAP sequences containing early stop codons at the 78th or 100th amino acid positions but otherwise WT in sequence conferred increases in AAV2 or AAV8 packaging levels.[42,43] To decouple whether any potentially improved functions of MAAP variants were due to their novel missense mutations and/or novel C-terminal domains, we generated the truncation variants L78* and L100* (MAAP-WT2 containing nonsense mutations at the 78th or 100th amino acid positions) as controls (Figure 4C; Table S1). We analyzed the effect of MAAP-SL01 and MAAP-SL08 provided in *trans* on the packaging of recombinant AAV2 encoding GFP. Specifically, recombinant AAV2 packaged by triple transfection of a plasmid encoding the GFP transgene flanked by AAV2 ITRs, pHelper, and pAAV2ΔMAAP in HEK293 cells stably expressing lentivirally delivered MAAP-SL01 or MAAP-SL08 exhibited statistically significant higher overall titer than production from cells stably expressing MAAP-WT2 (Figure 5A). Similarly, recombinant AAV2 packaged by triple transfection of a plasmid encoding the GFP transgene flanked by AAV2 ITRs, pHelper, and pAAV2 encoding WT AAV2 capsids (retaining expression of endogenous MAAP) in HEK293 cells stably expressing lentivirally delivered MAAP-SL08 exhibited statistically significant higher overall titer than production from cells lacking MAAP expression (Figure S6). Additionally, we investigated the infectious titer of the secreted AAV2ΔMAAP fractions following GFP packaging in cell lines stably expressing each MAAP variant. We divided the infectious titer by the vector genome titer to find the specific infectivity. Interestingly, secreted AAV2-ΔMAAP packaged in HEK293 cells stably expressing MAAP-SL08 variant in *trans* exhibited a higher specific infectivity relative to packaging in HEK293 cells expressing the MAAP-WT2 (Figure S7). Furthermore, a higher full/empty capsid ratio was observed for the lysate fraction of AAV2 ΔMAAP packaged in the presence of SL01 and SL08 (Figure S5). Taken together, these results indicate that MAAP variants resulting from directed evolution may be useful in industrially relevant AAV manufacturing processes.

MAAP variants isolated from AAV2 screens also enhance recombinant AAV6 and AAV9 packaging

We characterized whether the evolved MAAP variants showed cross-serotype activity for AAV6 or AAV9 packaging. First, we generated

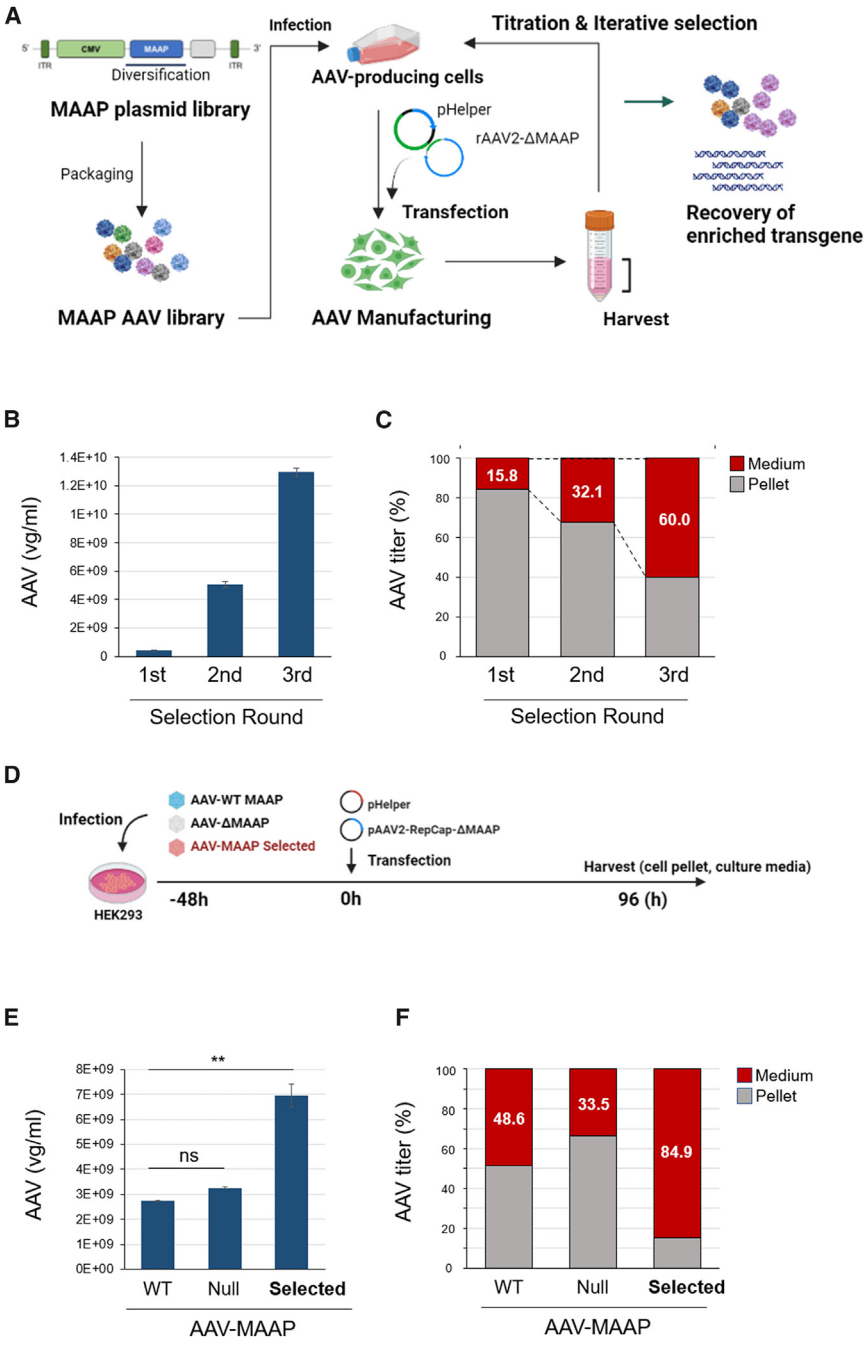

Figure 3. Directed evolution approach for MAAP

(A) Schematic of directed evolution approach to generate MAAP variants that confer improved AAV2 production in HEK293 cells. Created on BioRender.com. (B) Head-to-head comparison of total vector genome titer (obtained by qPCR) of the MAAP library bulk population after one, two, or three rounds of AAV2-MAAP-null packaging selection relative to the titer after the first round. (C) Ratio of secreted vector genomes for samples described in (B). (D) Schematic for head-to-head comparison of individual MAAP variants. Created on BioRender.com. (E) Head-to-head comparison of relative total vector genome titer (obtained by qPCR) when packaged into AAV2-MAAP-null containing WT MAAP2, no MAAP, or the selected MAAP library bulk population. (F) Ratio of secreted AAV2 for samples in (E). Error bars, mean ± SD. **p < 0.01 (Student's t test, two sampled).

AAV6 (AAV6ΔMAAP) or AAV9 (AAV9ΔMAAP) packaging plasmids for which the endogenous MAAP sequences were ablated by introducing a silent mutation into the near-cognate CTG start codon, which, like AAV2ΔMAAP, resulted in no change to the amino acid sequence produced by the VP1 ORF. A GFP transgene packaged into recombinant AAV6ΔMAAP or AAV9ΔMAAP by triple transfection in HEK293 cells stably expressing MAAP-SL08 was produced at statistically significant increased levels relative to HEK293 cells stably expressing MAAP-WT6 or MAAP-WT9, respectively (Figures 5B and 5C).

DISCUSSION

Discovered serendipitously as a contaminant of adenovirus preparations in 1965,[44,45] AAV is a rare example of a virus that has been extensively studied despite not being pathogenic in any known organism.[1,46] Despite AAV's short genome with a relatively small number of ORFs, many mechanisms underlying its biology are not well understood and, in some cases, are completely unknown. For example, the translocation of mature AAV particles away from the nucleus and egress out of the cell require additional investigation. Developing a clear understanding of these processes may improve manufacturing and therapeutic outcomes of AAV-based gene therapies. The discovery and characterization of MAAP illuminates AAV genomic mutations that may adversely or beneficially affect vector quality and yield. Encoded by an ORF that overlaps with the VP1-encoding ORF, MAAP and the viral VPs naturally co-evolved under strict evolutionary constraints. By uncoupling the ORF encoding MAAP from *cap*, such natural evolutionary constraints can be loosened to enable novel mutations, such as SNPs affecting highly conserved VP1 residues or frameshifts resulting in unique C-terminal domains, that would not be possible in a natural evolutionary context.

AAV-based gene therapies currently under clinical evaluation require high doses (as low as $\sim 1 \times 10^{10}$ vector genomes per patient for localized gene therapy applications and up to $\sim 1 \times 10^{17}$ vector genomes per patient for applications requiring systemic delivery)[47,48] to achieve a therapeutic effect. AAVs are currently utilized in 161 active- or

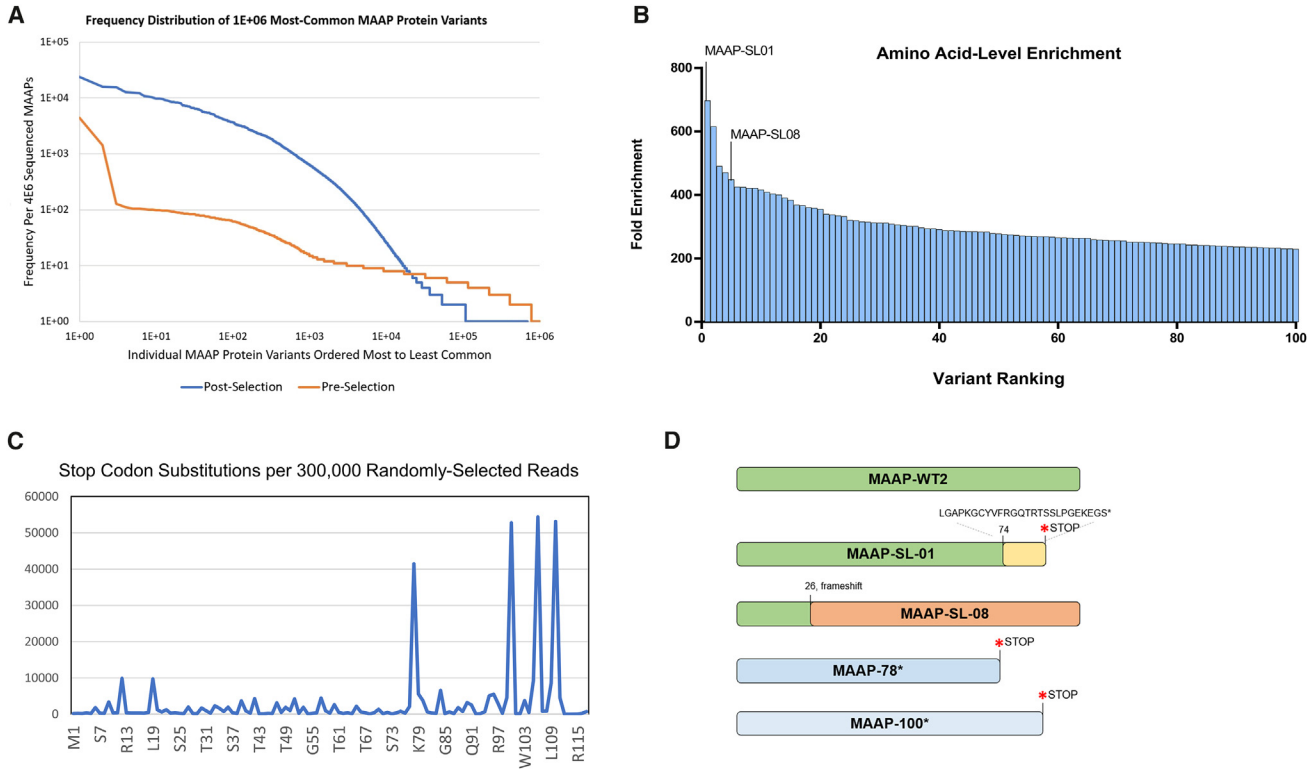

Figure 4. NGS of selected MAAP library uncovers strong enrichment of common features

(A) MAAP variants present in the pre-packaging (orange) or post-selection (blue) error-prone MAAP library were aligned, trimmed, translated into amino acid sequence, and ordered based on their frequency. The number of overall MAAP variant sequences with >1 read decreased by approximately one order of magnitude and leading MAAP variants increased in prevalence in the post-selected MAAP library population relative to the pre-packaging MAAP library population. (B) Quantitation of fold enrichment of the top 100 unique amino acid sequences present in the post-selection library population relative to the pre-packaging library population. Selected MAAP variants were named based on the order of their enrichment. (C) Early stop codons resulting in C-terminal truncations occurred frequently in the post-selected MAAP library population. (D) Schematic of MAAP-WT2, MAAP-WT2 truncated MAAP sequences (MAAP-L78* and MAAP-L100*), and two selected leading variants from our directed evolution process (MAAP-SL01 and MAAP-SL08).

recruiting status clinical trials as of May, 2023,[25] and robust preclinical research activity feeding the translational pipeline continues. Furthermore, preclinical and clinical exploration of AAV gene therapies have been expanding from CNS (including retinal) conditions, which in general require lower AAV doses,[49] to musculoskeletal and other conditions that require high vector doses.[50,51] Thus, manufacturing systems face tremendous hurdles to enable AAV gene therapy's full potential. To achieve sustainable scale-up in the face of increasing demand, innovations leading to higher per-cell output of functional recombinant AAV particles, increased secreted-to-pellet-retained ratios, and lowered full-to-empty and full-to-truncated vector ratios during upstream vector manufacturing processes will be needed.

Here, we report a directed evolution approach for generating MAAP variants that confer increased quality and quantity of AAV vectors (Figure 3). This approach generated two MAAP variants, MAAP-SL01 and MAAP-SL08, that confer increased GFP transgene packaging into AAV2 (Figure 5A). MAAP-SL08 also enabled statistically significant increases in GFP transgene packaging into AAV6 and AAV9, suggesting that MAAP-SL08 acts by mechanisms that are conserved across serotypes (Figures 5B and 5C). Although different seeding density, expression level, cell-line genotype, and temporal conditions of AAV packaging could conceivably modulate the effects of a given MAAP variant on AAV packaging output, MAAP-SL01 and MAAP-SL08 may have the potential to be directly applied to industrial-scale manufacturing processes. More broadly, our directed evolution approach may be applied to further optimize MAAP variants to any given manufacturing process or AAV serotype of interest.

MAAP-SL08 contains unanticipated features that could not have been predicted via rational engineering and whose underlying mechanisms will need to be further characterized. Specifically, MAAP-SL08 contained the first 26 amino acids of MAAP-WT2 followed by a frameshift into VP1 amino acid positions 54–196 with nine missense mutations scattered three to 20 amino acids apart (Figure 4D). Further work will need to be performed to determine whether improvements conferred by MAAP-SL08 are due to its missense mutations, VP1

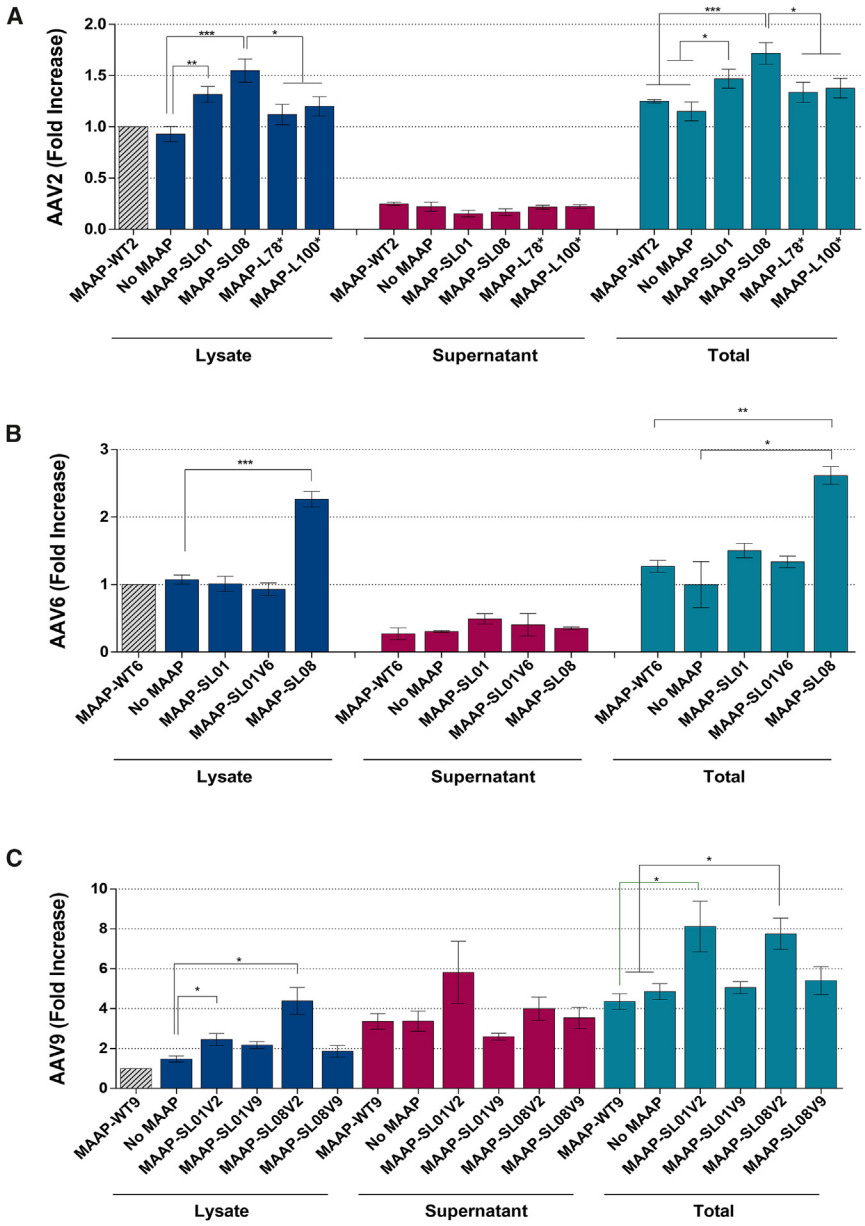

Figure 5. Selected MAAP variants confer increased vector genome packaging in AAV serotypes 2, 6, and 9

(A) GFP transgene packaging into AAV2 capsids (encoded by pAAV2ΔMAAP) in the presence of the indicated MAAP variant provided in *trans* via stable expression from the HEK293 cell genome. Media-associated, cell-associated, and total AAV titers for all conditions were normalized to the cell-associated titer of AAV packaged in MAAP-WT2 cells for each individual biological replicate (N = 10 independently packaged biological replicates). (B) GFP transgene packaging into AAV6 capsids (encoded by pAAV6ΔMAAP) in the presence of the indicated MAAP variant provided in *trans* via stable expression from the HEK293 cell genome. Media-associated, cell-associated, and total AAV titers for all conditions were normalized to the cell-associated titer of AAV produced in MAAP-WT6 cells for each individual biological replicate (N = 3). (C) GFP transgene packaging into AAV9 capsids (encoded by pAAV9ΔMAAP) in the presence of the indicated MAAP variant provided in *trans* via stable expression from the HEK293 cell genome. Media-associated, cell-associated, and total AAV titers for all conditions were normalized to the cell-associated titer of AAV packaged in MAAP-WT9 cells for each individual biological replicate (N = 3). Error bars, mean ± SEM. *p < 0.05, **p < 0.01, *** <0.005 (Student's t test, two sampled).

fusion region, or a combination thereof. Our second variant, MAAP-SL01 conferred statistically significant increases in AAV2 and AAV9 packaging (Figures 5A–5C). MAAP-SL01 contained the first 73 amino acids of MAAP-WT2, with the exceptions of 13 missense mutations, followed by a frameshift mutation that resulted in a novel 26 amino acid-long C-terminal domain (Figure 4D; Table S1). Hypotheses regarding the underlying mechanisms of how individual missense mutations, truncations, and C-terminal charge change affect AAV output deserve further experimental exploration.

Given the marked increase in secretion ratios observed in the bulk-selected library population vs. WT MAAP, it was an unanticipated finding that MAAP-SL01 and MAAP-SL08 drove higher overall vector genome titers without significantly increasing the titer of vector genomes secreted to the supernatant. Our observation that secreted AAV2-ΔMAAP packaged in HEK293 cells stably expressing the MAAP-SL08 variant in *trans* exhibited a modest increase in specific infectivity relative to secreted AAV2-ΔMAAP packaged in HEK293 cells expressing MAAP-WT2 or in the absence of MAAP (Figure S7) provides a potential explanation for how selection of secreted AAV enriched for MAAP variants that increased the cell-associated titer, as secreted variants with higher specific infectivity would be more likely to be taken up by neighboring cells rather than remain in the supernatant. That is, since our selective pressure involved transiently transfecting HEK293 cells with pHelper and Rep-Cap plasmids, along with a very low MOI of the MAAP library within infectious AAV to minimize the incidence of two MAAP variants infecting a single cell, the majority of cells likely took up the packaging plasmids but were initially not infected by an AAV. Cells infected with an AAV library member carrying a more fit MAAP variant, such as SL01 or SL08, may have secreted AAV with a higher specific infectivity than less fit MAAP variants. These higher-specific-infectivity AAVs would then be more likely to infect neighboring cells, many of which received packaging constructs but no AAV, leading to a second round of AAV

packaging. Multiple rounds of such packaging, secretion, and reinfection could have amplified variants such as SL01 and SL08 within the AAV population. It will be interesting for future studies to characterize the mechanism by which MAAP variants affected specific infectivity of secreted AAV, such as through altering the VP1/VP2/VP3 ratio and vector genomes. Additional possibilities explaining the striking observed increase in secreted AAV2 vector genomes conferred by the bulk-selected MAAP library population relative to MAAP-WT2 (Figure 3F) include the time point at which AAV was sampled following transfection of helper plasmids or that the selected library variants accounting for increase in secreted vector genomes remain unexplored within our dataset. Additional factors worth exploring include how temporal regulation and strength of MAAP expression levels affect AAV packaging. Our stable cell lines expressed MAAP constitutively under a CMV promoter, although it is possible that alternative or inducible promoters may further modulate effects.

In addition to our directed evolution approach and characterization of two leading individual evolved variants, we confirmed prior results, previously shown for AAV8,[43] that the knockout of MAAP from AAV2 (AAV2ΔMAAP) results in decreased AAV titer secreted in the supernatant when sampled 72 h post transfection (Figures 1A–1F). Our findings that the level of AAV2ΔMAAP associated with EVs is lower than that of WT AAV2, in addition to recent findings that MAAP associates with EVs,[43] further indicate that MAAP may play a role in incorporating AAV into EVs. MAAP8 was recently found to be important for EV association of AAVs but did not affect the size or number of EVs secreted into the medium. Our results in AAV2 closely corroborate this finding. An interesting future avenue would be to determine whether the AAV particles are physically enclosed within EVs or simply tethered to the outer surface of EVs.

More broadly, developing a deeper mechanistic understanding of the pathways and mechanisms that AAVs follow from capsid assembly and genome loading in the nucleus to nuclear escape, intracellular trafficking, and egress will enable engineering of more manufacturable and efficacious AAV gene therapies. The translation of improvements in AAV production to industrial settings can contribute to profound consequences of reducing global costs of and increasing patient access to these promising, life-saving medicines.

MATERIALS AND METHODS

Plasmids and viruses

For *pSubMAAP*, pX601 vector was digested with NcoI + BamHI (New England Biolabs, Ipswich, MA) at 37°C for 60 min. The MAAP-WT2 DNA sequence was isolated from the AAV2 genome by Q5 polymerase-based PCR (New England Biolabs, Ipswich, MA) and cloned into pSubMAAP to assess MAAP effects of MAAP knockout and reconstitution (Figures 1A–1F and 2A–2F). PCR products were purified using a PCR purification kit (Qiagen, Hilden, Germany) following the manufacturer's protocol, then digested with NcoI + BamHI at 37°C for 60 min. The digested PCR product and pSubMAAP vector were then ligated together using T4 DNA ligase (New England Biolabs, Ipswich, MA), transformed into Top10 competent cells (Thermo Fisher Scientific, Waltham, MA), and DNA was isolated and purified by midi prep (Thermo Fisher Scientific, Waltham, MA) following the manufacturer's protocol. Start codon of MAAP-WT2 (CTG) was substituted with ATG using the Q5 Site-Directed Mutagenesis Kit (New England Biolabs, Ipswich, MA) in accordance with the manufacturer's protocol.

pMAAP-Library

Error-prone PCR was used to amplify MAAP from the AAV2 genome following the staggered extension process previously described.[52] Briefly, 10× EP buffer (5 μL), differential volumes of 5 mM $MnCl_2$ (0, 0.2, 0.5, or 0.8 μL), DMSO (2.5 μL), 10× dNTPs (5 μL), 2.5 μL of each 10 μM primer (5′ [AJ005 sequence] 3′ and 5′ [AJ006 sequence] 3′), 1 μL of AAV2 genomes diluted to 1 ng/μL, Taq polymerase (1 μL), and water (30.5 μL) were mixed together and cycled 33 times as shown in Table S3 and run on a gel as shown in Figure S2. pSub MAAP was digested with NheI/SpeI in CutSmart buffer for 1.5 h at 37°C. EP PCR products (inserts) were run on 1.5% LMT agarose gel. The ∼370-bp band was excised, gel purified using a gel purification kit (Qiagen), digested using NheI/SpeI for 4 h, purified using AMPure XP beads, and ligated with the digested pSubMAAP vector at a 100 ng:37.5 ng vector:insert ratio using T4 DNA ligase (New England Biolabs, Ipswich, MA). The ligation reactions were desalted for 40 min using a membrane on molecular-grade H_20 and electroporated into DH10B electrocompetent cells. Electroporated cells were then grown up in overnight cultures and maxi prepped using the manufacturer's protocol (Thermo Fisher Scientific, Waltham, MA).

pAAV2ΔMAAP

A Q5 Site-Directed Mutagenesis Kit (New England Biolabs, Ipswich, MA) was used to mutate the 19th amino acid position, leucine (TTG), to a stop codon (TAG) in the MAAP ORF while introducing only a silent mutation in the 45th amino acid position, leucine (CTT→CTA) in the VP1 ORF of AAV2. Forward (5′GCAGGGGTCTaGTGCTTCCTG3′) and reverse (5′TGTCGTCCTTATGCCGCT3′) primers were used on pRepCap2 (described previously). The plasmid was functionally verified using triple transfection assay in HEK293 cells that successfully packaged AAV2 but produced no MAAP (Figure S1).

pAAV9ΔMAAP

A Q5 Site-Directed Mutagenesis Kit (New England Biolabs, Ipswich, MA) was used to mutate the first amino acid position, leucine (CTG), to a proline (CCG) in the MAAP ORF while introducing only a silent mutation in the 27th amino acid position, proline (CCT→CCC) in the VP1 ORF of AAV9. Unlike the near-cognate start codon CTG, transcriptional initiation from CCG codons is inefficient and rare in mammalian cells, as repeatedly shown through its infrequent occupation in ribosome profiling assays.[53–55] Primer sequences 5′-CTTTGAAACCcGGAGCCCCTC-3′ and 5′-CCCACCACTCGCGAATTC-3′ were used with pAAV9 as template, and the manufacturer's protocol was followed.

pAAV6ΔMAAP

In the same manner as pAAV9*ΔMAAP* generation, the Q5 Site-Directed Mutagenesis Kit (New England Biolabs, Ipswich, MA) was used to mutate the first amino acid position, leucine (CTG), to a proline (CCG) in the MAAP ORF while introducing only a silent mutation in the 27th amino acid position, proline (CCT → CCC) in the VP1 ORF of AAV6. Primer sequences 5′- ACTTGAAACCcGGAGCCC CGAAAC-3′ and 5′-CCCACCACTCGCGAATGC-3′ were used with pAAV6 as template, and the manufacturer's protocol was followed.

Lentivirus plasmids for stable cell line generation

pCW57 was digested with ClaI and BamHI. PCR of MAAP inserts was performed using pSubMAAP vectors for which the indicated MAAP variant had previously been incorporated (pSubMAAP-WT2, pSubMAAP-SL01, pSubMAAP-SL08, pSubMAAP-L78*, or pSubMAAP-L100*) as template. The PCR products were digested using ClaI and BamHI in 1× CutSmart buffer (New England Biolabs, Ipswich, MA) and ligated into the pCW57 backbone using T4 DNA ligase. Samples were transformed into Top10 bacterial cells, and an individual colony was selected and verified using Sanger sequencing.

Cell lines

Parental cells

HEK293 parental cells and HEK293T cells were obtained from the American Type Culture Collection (Manassas, VA, USA) and cultured in Dulbecco's modified Eagle's medium (DMEM, manufactured by Gibco) with 10% fetal bovine serum (FBS, manufactured by Invitrogen) and 1% penicillin/streptomycin/amphotericin B (GIBCO) at 37°C and 5% CO_2.

Lentivirus packaging

HEK293T cells (8×10^6 cells per dish) were passaged into 10-cm cell culture dishes. After 16 h of incubation, the HEK293T cells were transfected with third-generation lentivirus packaging plasmids using the following: DMEM (0.94 mL), lentivirus packaging plasmid with gene of interest (10 μg), pMDLg/pRRE (5 μg), RsRev (2.5 μg), VSV.G (2.5 μg), and PEI (60 g). Medium was changed 12 h post transfection, and HEPES was added at 20 mM final concentration. Following 48 h post transfection, supernatant was harvested in 15-mL conical tubes, centrifuged at 3,000 rpm for 5 min, and filtered using a 200-μm filter syringe unit. The remaining lysate was stored at −80°C for subsequent use.

Transduction and selection of cells stably expressing individual MAAP proteins

HEK293 parental cells (which do not contain T antigen) were plated into three full six-well plates (6×10^5 cells per well) and subsequently infected with packaged lentivirus with polybrene (8 μg/mL). Two days post transduction, the infection medium was replaced with selection medium containing puromycin (1 μg/mL). Cells were monitored and passaged until all non-infected cells were dead, at which point cells were amplified in 15-cm dishes, trypsinized, resuspended in DMEM containing 10% DMSO and 50% FBS, transferred to cryovials (Thermo Fisher Scientific, Waltham, MA), and frozen at −80°C for further use.

Verification and culture conditions for cells stably expressing individual MAAP proteins

HEK293 cells stably expressing MAAP proteins were thawed from −80°C and passaged in DMEM containing 10% FBS and 1% antibiotic-antimycotic (Thermo Fisher Scientific, Waltham, MA) at 37°C, 5% CO_2 five times before use. Cell viability was measured at passage number five using trypan blue (Figure S3A); cell lines were used for the first biological replicate of AAV2, AAV2ΔMAAP, AAV6ΔMAAP, or AAV9ΔMAAP packaging experiments; and stocks were frozen at −80°C for use in subsequent biological replicates. For RT-PCR (Figure S3B), total mRNA was isolated using RNeasy Plus kit (Qiagen, Hilden, Germany) and quantified mRNA was converted into cDNA using the iSelect cDNA synthesis kit (Bio-Rad, Hercules, CA) in accordance with the manufacturer's instruction. Synthesized cDNA was used for RT-PCR with specific primers targeting each MAAP WT or variants (MAAP-WT2 forward, 5′-ATGGCCCAC CACCACCAA-3′; WT2 reverse, 5′-GAAACTCCGCGTCGGCGT-3′; MAAP2-SL01 reverse, 5′-GCTGCCGGTCGTAGGCTT-3′; MAAP-WT6 forward, 5′-ATGGAGCCCCGAAACCCA-3′; MAAP-WT6 reverse, 5′-GCAGACGCTCCTGAAACTC-3′; MAAP-WT9 forward, 5′-GAGCCCCTCAACCCAAGGC-3′; MAAP-WT9 reverse, 5′-TCTT TGAGCCGCTCCTGGA-3′).

Selection of MAAP variants that confer increased AAV2 production

To select for MAAP variants that confer increase in AAV2 packaging production, the MAAP libraries were first packaged into rAAV2 (pMAAP-Library, pHelper, and pAAV2ΔMAAP) in parental HEK293 cells. At 96 h post infection (HPI), cell-associated or supernatant-associated AAV was sampled and titered via qPCR using the methods described below. The resulting supernatant-associated MAAP library packaged into AAV2 was then used to infect fresh parental HEK293 cells at MOI = 100, followed by co-transfection of pHelper and pAAV2ΔMAAP at 24 HPI. AAV was sampled at 96 HPI, and the supernatant-associated AAV was used to infect HEK293 cells at MOI = 100. After four iterations of this process, the total AAV was harvested and prepared for NGS.

NGS and bioinformatics

NGS of the pre- and post-selected MAAP library was performed to evaluate the fold enrichment of each MAAP sequence following execution of selections for AAV packaging and secretion to the cell culture medium. The MAAP sequence was amplified (forward primer, 5′ GCGCctggctaactaccggtgctagc-3′ and reverse primer, 5′-GCCAgtaatctggaacatcgtatgggtagActaGt-3′) from the AAV genomes following the fourth round of selection by PCR using Q5 High-Fidelity DNA polymerase (New England Biolabs, Ipswich, MA) and 21 cycles of PCR. PCR products were purified using AMPure XP beads (Beckman Coulter, Brea, CA) using the manufacturer's protocol. The resulting product was quantified using a Qubit dsDNA HS

assay kit and Qubit fluorometer (Thermo Fisher Scientific, Waltham, MA), and a total of 30 μg was used as template for 10 PCR cycles using IDT-8 TruSeq primers for barcoding. The barcoded amplicons were then pooled and sequenced at the QB3 Vincent J. Coates Genomics Sequencing Laboratory at University of California, Berkeley using the 300 PE MiSeq platform and TruSeq SBS Kit v3-HS (Illumina, San Diego, CA). Illumina FASTQ files were demultiplexed, and adaptor sequences were trimmed. The resulting demultiplexed sequences were analyzed using Geneious software (Dotmatics, Boston, MA) to determine the identity and read count of each MAAP sequence.

AAV packaging to assess MAAP variant function

Stable cell lines expressing selected variants of MAAP (sequences shown in Tables S1 and S2) were triple transfected using PEI with pHelper, AAV-Rep/Cap ΔMAAP, and the ss-CAG-GFP. At 4 days post transfection, supernatant and cells were harvested to determine AAV titer using detergent-based method as previously described.[56]

qPCR

To assess AAV titer in the supernatant, cell supernatant was collected at the indicated time point. Cell debris was removed by centrifugation at 3,000 rpm in a table-top centrifuge for 5 min. Next, $MgCl_2$ and Benzonase (Millipore, Hayward, CA) were added per milliliter of supernatant sample and incubated for 1 h at 37°C. After 1 h, Benzonase was neutralized by adding NaCl per milliliter of sample. Samples were then 10-fold diluted with deionized (DI) water and assayed by qPCR to quantify amounts of GFP transgene as described below. To assess AAV titer associated with the cell pellet, cell medium was replaced with 4 mL of DMEM containing 10% Triton X-100, Benzonase, and $MgCl_2$. Cells were then incubated for 1 h at 37°C and were rocked every 15 min. After 1 h, 1 mL of cell medium containing detached cells was collected and diluted 10-fold with DI water for subsequent qPCR analysis. qPCR was used to quantify the titer of AAV particles that contain genomes using SYBR Green, 3 mM $MgCl_2$, 0.2 mM dNTP, and Jump Start Taq on a CFX RT-PCR machine (Bio-Rad, Hercules, CA). Plasmid DNA was used from a concentration of 1 ng/μL to 0.0001 ng/μL to generate a standard curve with primers against CMV (5′-ATGGTGATGCGGTTTTGGCAG-3′ and 5′-GGC GGAGTTGTTACGACATTTTGG-3′) or GFP (5′-ACTACAACAG CCACAACGTCTA TATCA-3′ and 5′-GGCGGATCTTGAAGTTC ACC-3′). Each biological replicate represented a separately transfected T-25 flask, where the number of plates ranged from n = 3 to n = 6 performed on separate days. Each biological replicate was assayed with two technical replicates during qPCR analysis.

Capsid quantification

Fully assembled capsids of AAV2 were quantified using sandwich ELISA (PROGEN, AAV Titration ELISA 2.0R) according to manufacturer's protocol. Each sample from the lysate or supernatant was diluted 200-fold and analyzed using ELISA reader at wavelength 450 nm (Bio-Tek uQUANT Microplate Spectrophotometer). Viral genome copy number of each sample was normalized to capsid quantification to calculate the full and empty capsid ratio.

Immunoblot analysis

HEK293T cells were transfected with pSubMAAP using PEI. At 36-h post transfection, cells were harvested and lysed with RIPA buffer (20 mM Tris-HCl, pH 7.4, 150 mM NaCl, 1% NP-40, and 1 mM EDTA) containing a protease inhibitor cocktail (Thermo Fisher Scientific, Waltham, MA). Whole-cell lysates were loaded into pre-prepared SDS-PAGE gel (Invitrogen, Waltham, MA) and transferred to polyvinylidene fluoride (PVDF) membrane. Anti-hemagglutinin (HA) antibody (Cell Signaling, #3724) (1:1,000), anti-GAPDH antibody (Cell Signaling, #2118) (1:1,000), and horseradish peroxidase (HRP)-conjugated anti-rabbit IgG antibody (Cell Signaling, #7074) (1:3,000) were used for immunoblotting.

Extracellular vesicle isolation and quantification

We harvested supernatant from HEK293T cells grown in DMEM supplemented with 10% FBS and conditioned to remove pre-existing EVs in seven 15-cm cell culture dishes (Thermo Fisher Scientific, Waltham, MA). All subsequent manipulations were completed at 4°C. Cells and large debris were removed by low-speed sedimentation at 1,000 × *g* for 15 min followed by medium-speed sedimentation at 10,000 × *g* for 15 min in an F10-6X500Y rotor (Sorvall). EVs were pelleted from conditioned medium by spinning at ∼100,000 × *g* (29,500 rpm) for 1 h in an SW32 Ti rotor (Beckman), and the supernatant was discarded. Crude EVs were resuspended in PBS. Resuspended crude EVs were spun at 1,000 × *g* for 5 min to remove any aggregates formed during centrifugation. A solution of 65% sucrose, 20 mM Tris pH 7.4 were added to resuspended crude EVs until the solution reached 55% sucrose, and 3 mL of this solution was added to an SW55 tube. Next, 1 mL of 40% sucrose, 20 mM Tris pH 7.4 followed by 1 mL of 10% sucrose, 20 mM Tris pH 7.4 was carefully layered onto the gradient and centrifuged in an SW55 rotor (Beckman) at 36,500 rpm for 16 h with minimum acceleration and no brake. Fractions (400 μL) were collected from top to bottom and analyzed by western blot (Figure 2B; Figure S4). Density measurements were taken using a refractometer.

Infectious titer

To assess AAV titer in the supernatant, cell supernatant was collected at the indicated time point. Cell debris was removed by centrifugation at 3,000 rpm in a table-top centrifuge for 5 min. Next, $MgCl_2$ and Benzonase (Millipore, Hayward, CA) were added per milliliter of supernatant sample and incubated for 1 h at 37°C. After 1 h, Benzonase was neutralized by adding NaCl per milliliter of sample. Samples were then 10-fold diluted with DMEM containing 4% FBS and infected onto HEK293 cells for 12 h, at which point the medium was replaced with fresh DMEM containing 4% FBS. Four days post infection, HEK293 cells were trypsinized, rinsed with 1× PBS, fixed in paraformaldehyde (PFA), and analyzed on an Attune flow cytometer for GFP-expressing cells. The percentage of GFP-expressing cells was multiplied by the dilution factor to obtain an infectious titer value for each sample. To calculate specific infectivity, the infectious titer was divided by the vector genome titer.

Statistical analysis

Raw data were recorded electronically and statistical analyses were performed with Microsoft Excel or Prism software version 9 (GraphPad Software, San Diego, CA). Vector titers were expressed as means ± SEM with Student's t test. All t tests depicted in this manuscript were comparing two samples. An α value (p) of 0.05 was considered as statistically significant, and all p values were two sided.

DATA AND CODE AVAILABILITY

All raw data, such as Excel documents containing qPCR and flow cytometry readouts or NGS datasets, are openly available upon request.

SUPPLEMENTAL INFORMATION

Supplemental information can be found online at https://doi.org/10.1016/j.ymthe.2023.12.015.

ACKNOWLEDGMENTS

We acknowledge Prof. Randy Schekman for sharing his helpful insights on EVs and Juan Hurtado for his consultation regarding NGS analysis. Research reported in this publication was supported by the National Institutes of Health under award numbers UF1MH130700 and R01NS126397.

AUTHOR CONTRIBUTIONS

A.J.S. co-conceived of the study design, contributed to all performed experiments, analyzed data, and wrote the manuscript. H.L. co-conceived of the study design, contributed to all performed experiments, analyzed data, and edited the manuscript. A.C. and V.K. contributed to cloning, stable cell line generation and maintenance, and assessment of infectious titer. J.K.W. performed EV sampling and the analysis depicted in Figures 2A–2F. D.V.S. supervised the project, co-conceived the study design, and edited the manuscript.

DECLARATION OF INTERESTS

A.J.S., H.L., and D.V.S. are inventors on a patent related to MAAP variants for increased production of recombinant AAV.

REFERENCES

1. Howley, P.M., Knipe, D.M., Cohen, J.L., and Damania, B.A. Fields Virology: DNA Viruses 7th edition Wolters Kluwer Health.
2. Li, C., and Samulski, R.J. (2020). Engineering adeno-associated virus vectors for gene therapy. Nat. Rev. Genet. *21*, 255–272.
3. Ogden, P.J., Kelsic, E.D., Sinai, S., and Church, G.M. (2019). Comprehensive AAV capsid fitness landscape reveals a viral gene and enables machine-guided design. Science *366*, 1139–1143.
4. Berthet, C., Raj, K., Saudan, P., and Beard, P. (2005). How adeno-associated virus Rep78 protein arrests cells completely in S phase. Proc. Natl. Acad. Sci. USA *102*, 13634–13639.
5. Schmidt, M., Afione, S., and Kotin, R.M. (2000). Adeno-associated virus type 2 Rep78 induces apoptosis through caspase activation independently of p53. J. Virol. *74*, 9441–9450.
6. Weger, S., Wendland, M., Kleinschmidt, J.A., and Heilbronn, R. (1999). The Adeno-Associated Virus Type 2 Regulatory Proteins Rep78 and Rep68 Interact with the Transcriptional Coactivator PC4. J. Virol. *73*, 260–269.
7. Hermonat, P.L., Santin, A.D., Batchu, R.B., and Zhan, D. (1998). The adeno-associated virus Rep78 major regulatory protein binds the cellular TATA-binding protein in vitro and in vivo. Virology *245*, 120–127.
8. Smith, R.H., Spano, A.J., and Kotin, R.M. (1997). The Rep78 gene product of adeno-associated virus (AAV) self-associates to form a hexameric complex in the presence of AAV ori sequences. J. Virol. *71*, 4461–4471.
9. Li, Z., Brister, J.R., Im, D.-S., and Muzyczka, N. (2003). Characterization of the adenoassociated virus Rep protein complex formed on the viral origin of DNA replication. Virology *313*, 364–376.
10. Tratschin, J.D., Miller, I.L., and Carter, B.J. (1984). Genetic analysis of adeno-associated virus: properties of deletion mutants constructed in vitro and evidence for an adeno-associated virus replication function. J. Virol. *51*, 611–619.
11. King, J.A., Dubielzig, R., Grimm, D., and Kleinschmidt, J.A. (2001). DNA helicase-mediated packaging of adeno-associated virus type 2 genomes into preformed capsids. EMBO J. *20*, 3282–3291.
12. Steinbach, S., Wistuba, A., Bock, T., and Kleinschmidt, J.A. (1997). Assembly of adeno-associated virus type 2 capsids in vitro. J. Gen. Virol. *78*, 1453–1462.
13. Mietzsch, P., Pénzes, J.J., and Agbandje-McKenna, M. (2019). Twenty-Five Years of Structural Parvovirology. Viruses *11*, 362.
14. Sonntag, F., Schmidt, K., and Kleinschmidt, J.A. (2010). A viral assembly factor promotes AAV2 capsid formation in the nucleolus. Proc. Natl. Acad. Sci. USA *107*, 10220–10225.
15. Maurer, A.C., Pacouret, S., Cepeda Diaz, A.K., Blake, J., Andres-Mateos, E., and Vandenberghe, L.H. (2018). The Assembly-Activating Protein Promotes Stability and Interactions between AAV's Viral Proteins to Nucleate Capsid Assembly. Cell Rep. *23*, 1817–1830.
16. Grosse, S., Penaud-Budloo, M., Herrmann, A.-K., Börner, K., Fakhiri, J., Laketa, V., Krämer, C., Wiedtke, E., Gunkel, M., Ménard, L., et al. (2017). Relevance of Assembly-Activating Protein for Adeno-associated Virus Vector Production and Capsid Protein Stability in Mammalian and Insect Cells. J. Virol. *91*, e011988-17.
17. Hermonat, P.L., Santin, A.D., De Greve, J., De Rijcke, M., Bishop, B.M., Han, L., Mane, M., and Kokorina, N. (1999). Chromosomal latency and expression at map unit 96 of a wild-type plus adeno-associated virus (AAV)/Neo vector and identification of p81, a new AAV transcriptional promoter. J. Hum. Virol. *2*, 359–368.
18. Cao, M., You, H., and Hermonat, P.L. (2014). The X Gene of Adeno-Associated Virus 2 (AAV2) Is Involved in Viral DNA Replication. PLoS ONE *9*, e104596.
19. Meier, A.F., Fraefel, C., and Seyffert, M. (2020). The Interplay between Adeno-Associated Virus and Its Helper Viruses. Viruses *12*, 662.
20. Geoffroy, M.C., and Salvetti, A. (2005). Helper functions required for wild type and recombinant adeno-associated virus growth. Curr. Gene Ther. *5*, 265–271.
21. Buller, R.M., Janik, J.E., Sebring, E.D., and Rose, J.A. (1981). Herpes Simplex Virus Types 1 and 2 Completely Help Adenovirus-Associated Virus Replication. J. Virol. *40*, 241–247.
22. Nahreini, P., Woody, M.J., Zhou, S.Z., and Srivastava, A. (1993). Versatile adeno-associated virus 2-based vectors for constructing recombinant virions. Gene *124*, 257–262.
23. Dismuke, D.J., Tenenbaum, L., and Samulski, R.J. (2013). Biosafety of recombinant adeno-associated virus vectors. Curr. Gene Ther. *13*, 434–452.
24. George, L.A., Ragni, M.V., Rasko, J.E.J., Raffini, L.J., Samelson-Jones, B.J., Ozelo, M., Hazbon, M., Runowski, A.R., Wellman, J.A., Wachtel, K., et al. (2020). Long-Term Follow-Up of the First in Human Intravascular Delivery of AAV for Gene Transfer: AAV2-hFIX16 for Severe Hemophilia B. Mol. Ther. *28*, 2073–2082.
25. (2023). clinicaltrials.gov (U.S. National Library of Medicine).
26. Sehara, Y., Fujimoto, K.I., Ikeguchi, K., Katakai, Y., Ono, F., Takino, N., Ito, M., Ozawa, K., and Muramatsu, S.I. (2017). Persistent Expression of Dopamine-Synthesizing Enzymes 15 Years After Gene Transfer in a Primate Model of Parkinson's Disease. Hum. Gene Ther. Clin. Dev. *28*, 74–79.
27. Sabatino, D.E., Bushman, F.D., Chandler, R.J., Crystal, R.G., Davidson, B.L., Dolmetsch, R., Eggan, K.C., Gao, G., Gil-Farina, I., Kay, M.A., et al. (2022). Evaluating the state of the science for adeno-associated virus integration: An integrated perspective. Mol. Ther. *30*, 2646–2663.

28. Chahal, P.S., Schulze, E., Tran, R., Montes, J., and Kamen, A.A. (2014). Production of adeno-associated virus (AAV) serotypes by transient transfection of HEK293 cell suspension cultures for gene delivery. J. Virol. Methods *196*, 163–173.

29. Negrete, A., and Kotin, R.M. (2008). Strategies for manufacturing recombinant adeno-associated virus vectors for gene therapy applications exploiting baculovirus technology. Brief. Funct. Genomic Proteomic. *7*, 303–311.

30. Rayaprolu, V., Kruse, S., Kant, R., Venkatakrishnan, B., Movahed, N., Brooke, D., Lins, B., Bennett, A., Potter, T., McKenna, R., et al. (2013). Comparative Analysis of Adeno-Associated Virus Capsid Stability and Dynamics. J. Virol. *87*, 13150–13160.

31. Bernaud, J., Rossi, A., Fis, A., Gardette, L., Aillot, L., Büning, H., Castelnovo, M., Salvetti, A., and Faivre-Moskalenko, C. (2018). Characterization of AAV vector particle stability at the single-capsid level. J. Biol. Phys. *44*, 181–194.

32. Podsakoff, G., Wong, K.K., and Chatterjee, S. (1994). Efficient gene transfer into nondividing cells by adeno-associated virus-based vectors. J. Virol. *68*, 5656–5666.

33. Ellis, B.L., Hirsch, M.L., Barker, J.C., Connelly, J.P., Steininger, R.J., and Porteus, M.H. (2013). A survey of ex vivo/in vitro transduction efficiency of mammalian primary cells and cell lines with Nine natural adeno-associated virus (AAV1-9) and one engineered adeno-associated virus serotype. Virol. J. *10*, 74.

34. Bartel, M.A., Weinstein, J.R., and Schaffer, D.V. (2012). Directed evolution of novel adeno-associated viruses for therapeutic gene delivery. Gene Ther. *19*, 694–700.

35. (2019). Approved Cellular and Gene Therapy Products: ZOLGENSMA (U.S. Food & Drug Administration)).

36. (2017). Approved Cellular and Gene Therapy Products: LUXTURNA (U.S. Food & Drug Administration)).

37. (2022). Approved Cellular & Gene Therapy Products: HEMGENIX (U.S. Food & Drug Administration)).

38. (2023). Approved Cellular and Gene Therapy Products: ELEVIDYS (U.S. Food & Drug Administration)).

39. (2023). Approved Cellular and Gene Therapy Products: ROCTAVIAN (U.S. Food & Drug Administration)).

40. Technology developments in viral vector manufacturing for cell and gene therapies store. Frost.com. https://store.frost.com/technology-developments-in-viral-vector-manufacturing-for-cell-and-gene-therapies.html.

41. Kolata, G. (2017). Gene Therapy Hits a Peculiar Roadblock: A Virus Shortage.

42. Galibert, L., Hyvönen, A., Eriksson, R.A.E., Mattola, S., Aho, V., Salminen, S., Albers, J.D., Peltola, S.K., Weman, S., Nieminen, T., et al. (2021). Functional roles of the membrane-associated AAV protein MAAP. Sci. Rep. *11*, 21698.

43. Elmore, Z.C., Patrick Havlik, L., Oh, D.K., Anderson, L., Daaboul, G., Devlin, G.W., Vincent, H.A., and Asokan, A. (2021). The membrane associated accessory protein is an adeno-associated viral egress factor. Nat. Commun. *12*, 6239.

44. Atchison, R.W., Casto, B.C., and Hammon, W.M.D. (1965). Adenovirus-Associated Defective Virus Particles. Science *149*, 754–756.

45. Hoggan, M.D., Blacklow, N.R., and Rowe, W.P. (1966). Studies of small DNA viruses found in various adenovirus preparations: physical, biological, and immunological characteristics. Proc. Natl. Acad. Sci. USA *55*, 1467–1474.

46. Hastie, E., and Samulski, R.J. (2015). Adeno-Associated Virus at 50: A Golden Anniversary of Discovery, Research, and Gene Therapy Success—A Personal Perspective. Hum. Gene Ther. *26*, 257–265.

47. Clément, N., and Grieger, J.C. (2016). Manufacturing of recombinant adeno-associated viral vectors for clinical trials. Mol. Ther. Methods Clin. Dev. *3*, 16002.

48. Au, H.K.E., Isalan, M., and Mielcarek, M. (2021). Gene Therapy Advances: A Meta-Analysis of AAV Usage in Clinical Settings. Front. Med. *8*, 809118.

49. Zhu, D., Schieferecke, A.J., Lopez, P.A., and Schaffer, D.V. (2021). Adeno-Associated Virus Vector for Central Nervous System Gene Therapy. Trends Mol. Med. *27*, 524–537. S1471491421000952.

50. Mendell, J.R., Al-Zaidy, S.A., Rodino-Klapac, L.R., Goodspeed, K., Gray, S.J., Kay, C.N., Boye, S.L., Boye, S.E., George, L.A., Salabarria, S., et al. (2021). Current Clinical Applications of In Vivo Gene Therapy with AAVs. Mol. Ther. *29*, 464–488.

51. Mendell, J.R., Sahenk, Z., Lehman, K., Nease, C., Lowes, L.P., Miller, N.F., Iammarino, M.A., Alfano, L.N., Nicholl, A., Al-Zaidy, S., et al. (2020). Assessment of Systemic Delivery of rAAVrh74.MHCK7.micro-dystrophin in Children With Duchenne Muscular Dystrophy: A Nonrandomized Controlled Trial. JAMA Neurol. *77*, 1122–1131.

52. Maheshri, N., Koerber, J.T., Kaspar, B.K., and Schaffer, D.V. (2006). Directed evolution of adeno-associated virus yields enhanced gene delivery vectors. Nat. Biotechnol. *24*, 198–204.

53. Cao, X., and Slavoff, S.A. (2020). Non-AUG start codons: Expanding and regulating the small and alternative ORFeome. Exp. Cell Res. *391*, 111973.

54. Kearse, M.G., and Wilusz, J.E. (2017). Non-AUG translation: a new start for protein synthesis in eukaryotes. Genes Dev. *31*, 1717–1731.

55. Hinnebusch, A.G. (2011). Molecular Mechanism of Scanning and Start Codon Selection in Eukaryotes. Microbiol. Mol. Biol. Rev. *75*, 434–467. first page of table of contents.

56. Dias Florencio, G., Precigout, G., Beley, C., Buclez, P.-O., Garcia, L., and Benchaouir, R. (2015). Simple downstream process based on detergent treatment improves yield and in vivo transduction efficacy of adeno-associated virus vectors. Mol. Ther. Methods Clin. Dev. *2*, 15024.